Note: Artificial neural networks for the automated analysis of force map data in atomic force microscopy

Christoph Braunsmann and Tilman E. Schäffer[a)]
Institute of Applied Physics and LISA+, University of Tübingen, Auf der Morgenstelle 10, 72076 Tübingen, Germany

(Received 7 April 2014; accepted 2 May 2014; published online 21 May 2014)

Force curves recorded with the atomic force microscope on structured samples often show an irregular force versus indentation behavior. An analysis of such curves using standard contact models (e.g., the Sneddon model) would generate inaccurate Young's moduli. A critical inspection of the force curve shape is therefore necessary for estimating the reliability of the generated Young's modulus. We used a trained artificial neural network to automatically recognize curves of "good" and of "bad" quality. This is especially useful for improving the analysis of force maps that consist of a large number of force curves. © *2014 AIP Publishing LLC*. [http://dx.doi.org/10.1063/1.4876485]

The atomic force microscope (AFM) is widely used for measuring mechanical sample properties. For this purpose, a force-versus-indentation-curve ("force curve") is recorded by pushing the tip of the AFM cantilever into the sample until a preselected trigger force is reached. A subsequent force curve analysis then allows a determination of the local Young's modulus of the sample.[1] In the force mapping mode, many force curves are recorded on distinct points of a preselected raster across the sample surface,[2–4] which allows creating images of the Young's modulus and the sample topography.

The commonly used contact models of Hertz[5] or Sneddon[6] are valid for the elastic indentation into a flat, homogenous, and infinitely thick sample. Unfortunately, these requirements are usually not fully fulfilled when examining nanostructured systems such as polymer nanocomposites,[7] cells,[2] or biological tissues.[4] A finite sample thickness or a structured surface may result in a force curve, whose shape significantly deviates from the prediction by the used contact model. A fit of this model would therefore produce inaccurate results.[8,9] A critical look at the shape of the recorded force curve is thus important to estimate the reliability of the measurement. Since force mapping may generate a large number of force curves (e.g., $64 \times 64 = 4096$ force curves), it is necessary to inspect the force curves automatically using a computer-based routine. We have previously shown that the average squared deviation of the fit from the data can be used for this purpose.[4] Here, we present another method that is based on pattern recognition by artificial neural networks and allows detecting force curves of "good" and "bad" quality in AFM force maps ("good" and "bad" curves, respectively).

To demonstrate the new method, we recorded a force map on the replica of an AFM calibration grid (MIKROMASCH TGX01, Innovative Solutions Bulgaria Ltd., Sofia, Bulgaria). The replica was made from a silicone elastomer (Sylgard® 186 Silicone Elastomer Kit, Dow Corning, Midland, USA). The force mapping measurements were performed using a commercial AFM (MFP-3D, Asylum Research, Santa Barbara, USA) and a standard cantilever (PPP-NCHR, NanoWorld, Neuchâtel, Switzerland, half cone angle ≈20°). The cantilever spring constant was calibrated using the thermal noise method.[10] Sneddon's contact model for conical tips[6] was applied to evaluate the local Young's modulus of the sample by using customized software written in Igor Pro (Wavemetrics, Lake Oswego, Oregon, USA). For details concerning the Young's modulus analysis see, e.g., Ref. 3.

The trigger height image (i.e., the z-positions at the trigger force) [Fig. 1(a)] shows the typical chessboard-like structure of the grid with a pitch of 3 μm and a structure height of ≈800 nm. Although the replica consists of a homogenous material, the grid structure appears in the Young's modulus image [Figure 1(b)]. Moduli in between 1.5 and 2.5 MPa (red-yellow color) were measured on the flat regions of the grid (two height levels). In contrast, moduli in between 0.5 and 1.5 MPa (blue color) were measured at the edges in between the two height levels. Figure 1(c) shows several force curves from the recorded map. Force curves 1 and 2 were recorded on the flat areas of the grid and show clearly recognizable non-contact (indentation <0) and contact (indentation >0) parts. The fit of Sneddon's contact model (black dashed traces) matched the data very well and thus gave a reliable value for the local Young's modulus. However, force curves 3 and 4, which were recorded at the edges of the grid, showed an irregular force curve shape with several kinks in the contact part. These kinks indicated that the tip end slipped off the edges of the grid due to a poorly defined tip-sample contact. Consequently, the fit of Sneddon's model did not match the recorded data and the evaluated Young's moduli are certainly not reliable. The histogram of the Young's modulus [Fig. 1(d)] showed a rather broad distribution of values with peaks at about 1 MPa and at about 1.8 MPa.

To improve the quality of the Young's modulus measurement we implemented an artificial neural network in our analysis routine, which was trained to detect force curves with an irregular shape that clearly deviated from the one predicted by Sneddon's contact model [="bad" force curves, Fig. 2(a)]. The used neural network (a three layer perceptron[11]) consisted of an input layer with 100 nodes, a hidden layer with

[a)]Author to whom correspondence should be addressed. Electronic mail: tilman.schaeffer@uni-tuebingen.de.

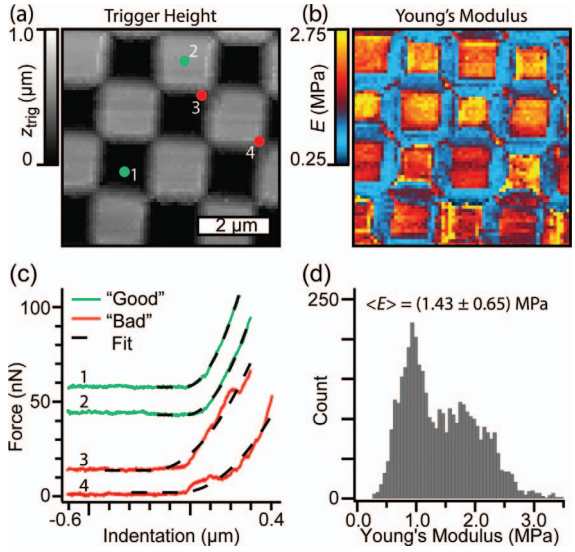

FIG. 1. Force map recorded on a replica of an AFM calibration grid made from a silicone elastomer (trigger force 50 nN, 64 × 64 force curves). (a) Trigger height image. (b) Young's modulus image. The structure of the grid replica is clearly visible, although the grid was made from a homogenous material. (c) Force curves recorded on flat surface areas (green) and at the edges of the grid structures (red). Curves 1– 3 were vertically shifted for better visibility. (d) Histogram of the Young's modulus image.

five nodes, and an output layer consisting of a single node [Fig. 2(b)]. The interconnection between a node i of one layer with a node j of the following layer was characterized by the weight parameter w_{ij}. The output of node j (a hidden layer node or the output node) ranged in between 0 and 1 and was calculated by the nonlinear activation function:

$$V_j = \left[1 + \exp\left(-\sum_{i=1}^{n} w_{ij} s_i\right)\right]^{-1}. \quad (1)$$

Here, the s_i were the inputs from node i in the upper layer and n was the number of inputs connected to node j ($n = 100$ for a hidden layer node and $n = 5$ for the output node). The force curve was first normalized to a data range in between 0 and 1 to obtain a comparable set of data that can be processed by the neural network. Afterwards, the number of force curve data points (≈700) was normalized by interpolation to 100. The 100 consecutive values of the normalized force curve represented the s_i values of the 100 input nodes. A number of five hidden layer nodes were chosen, since networks with more or fewer hidden layer nodes usually gave a worse performance (a larger number of false decisions).

The neural network was trained with a data set consisting of "good" and "bad" force curves, which were associated with an output node activation of 1 or 0, respectively ("supervised learning"[11]). To create such a training data set, we first manually selected 50 curves with an irregular shape from the force map ("bad" curves) [Fig. 2(c)]. The "good" curves were not directly taken from the force map data because their average slope in the contact part was similar. This was because the sample consisted of a single material. An artificial neural network that is only trained with "good" force curves from the force map therefore possibly judges the force curve quality from its average slope and not from its irregular shape.

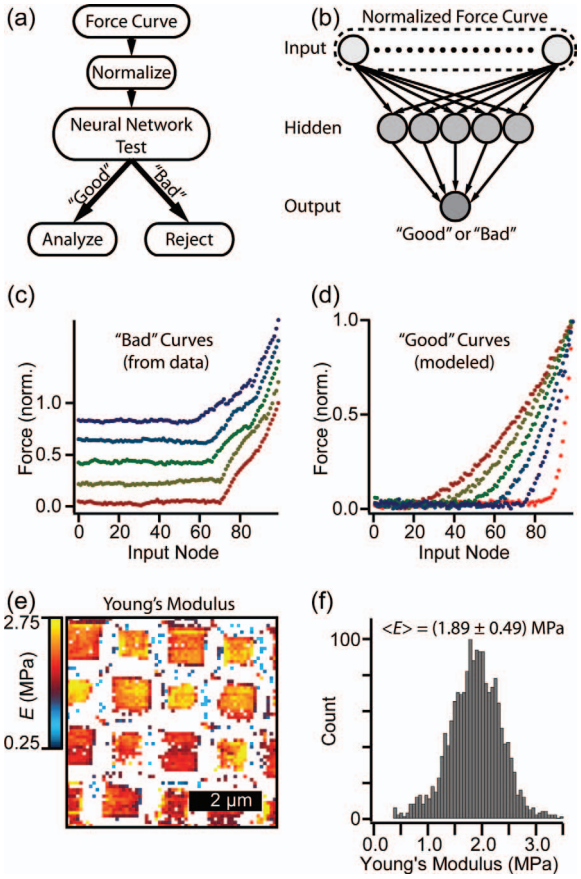

FIG. 2. (a) Flow chart describing the neural network test for detecting "good" and "bad" curves in the force map. (b) Structure of the used artificial neural network (a three layer perceptron). The network was trained with a data set consisting of "good" and "bad" force curves. (c) Normalized "bad" curves, taken from the force map data. The curves were vertically shifted for better visibility. (d) Normalized "good" curves that were modeled according to Sneddon's contact model. (e) Young's modulus image after rejecting all "bad" force curves. (f) Histogram of the Young's modulus image.

To prevent this, we modeled 100 "good" force curves showing a broad range of sample Young's modulus according to Sneddon's contact model and added them to the training data set [contact point node number varied in between 15 and 90, Fig. 2(d)]. The root-mean-square (RMS) noise in the recorded force curves was ≈250 pN, which is ≈0.5 % of the trigger force (50 nN). To ensure that the neural network did not reject "good" but slightly noisy curves from further analysis, we added a similar amount of Gaussian noise to the normalized model curves (standard deviation of Gaussian noise = 0.05).

The training algorithm was based on back-propagation and iteratively minimized the RMS error between the calculated and the preselected output node activations of the training data set by changing the weights w_{ij}.[11] After a number of 100 000 iterations, the RMS-error had decreased from a value close to 1 (almost no curve of the training set was properly judged) to a value smaller than 0.005 (all curves of the training set were judged correctly).

We next implemented the trained neural network in the analysis. Force curves that produced a neural network output node activation <0.9 showed an irregular shape (="bad" force curve) and were therefore rejected from the Young's

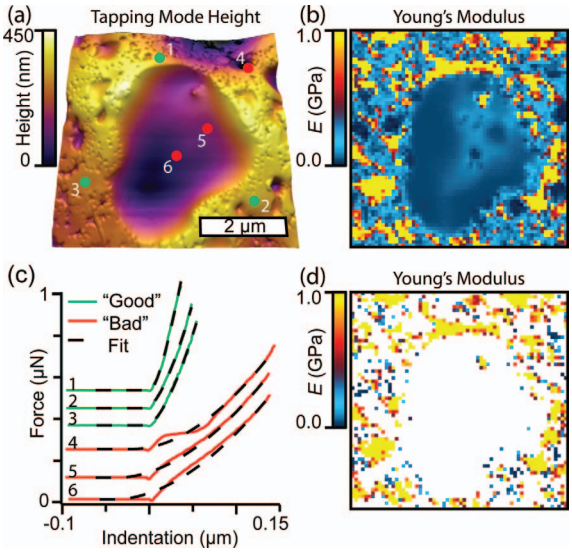

FIG. 3. Using a neuronal network on an epoxy adhesive to test whether this material obeys a Sneddon-like behavior. (a) 3D-rendered tapping mode height image. (b) Young's modulus image of a force map recorded on the same area as shown in (a) (trigger force 500 nN, 64 × 64 force curves). (c) Force curves recorded at positions 1–6, marked by green and red dots in (a). Curves 1–5 were vertically shifted for better visibility. (d) Young's modulus image after rejecting all "bad" force curves. Force map data from Ref. 12.

modulus image shown in Fig. 2(e) (white pixels). Most rejected force curves were located at the edges of the grid structures, but some were located on the flat regions. The histogram of the Young's modulus when rejecting all "bad" curves from the analysis consisted of only one peak around (1.89 ± 0.49) MPa [mean ± standard deviation, Fig. 2(f)]. A single peak was expected, since the grid replica consisted of a single homogeneous material. In contrast, a Young's modulus of (1.43 ± 0.65) MPa had been found when considering also the "bad" curves [Fig. 1(d)]. Including the trained neural network in the force map analysis therefore increased the measured average Young's modulus of the sample by 32% and reduced the relative error of this measurement from 45% to 26 %.

As a further example, we implemented a neural network in the analysis of a force map, which was recorded on the surface of an epoxy adhesive (Toolcraft Multi Power, distributed by Conrad Electronic SE, Hirschau, Germany). The tapping mode height image acquired before the force map reveals a large central and numerous smaller peripheral depressions with a depth of 100–400 nm [Fig. 3(a)]. The Young's modulus image shows large local variations ranging from about 50 MPa (dark blue) to about 1 GPa (yellow) [Fig. 3(b)]. A selection of six force curves recorded on different positions on the epoxy surface is shown in Fig. 3(c) [positions marked by numbered green and red dots in panel (a)]. Force curves 1–4 were recorded outside the large central depression. Curves 1–3 showed a shape that is well matched by a fit of Sneddon's contact model. In contrast, curve 4 clearly deviated from the fit. This can be explained by a poorly defined tip-sample contact at position 4, which lies on the boundary of a depression. Force curves 5 and 6 were recorded within the large central depression, which was basically flat. Nevertheless, the fits deviated significantly from the force curves. This deviation may be a consequence of the viscoelastic and plastic sample properties of the epoxy sample, which cannot be described by Sneddon's contact model. Implementing a neural network that was trained the same way as described above allowed rejecting all "bad" force curves, which did not follow a Sneddon-like behavior [Fig. 3(d), white pixels]. About 75% of all force curves were rejected by the neural network, showing that Sneddon's contact model cannot correctly describe the mechanical properties of the epoxy sample. We have shown before that the use of a force step load protocol in combination with an analysis based on the (viscoelastic) standard linear solid model provides a better way to characterize the mechanical properties of this epoxy.[12]

In summary, we demonstrated that force maps may contain "bad" force curves that do not show the force versus indentation behavior predicted by a chosen contact model. To obtain more reliable results, such curves must be excluded from further analysis. We showed that artificial neural networks can be trained to distinguish between "good" and "bad" curves, simplifying the analysis of large data sets.

[1]N. A. Burnham and R. J. Colton, J. Vac. Sci. Technol. A **7**(4), 2906–2913 (1989).
[2]M. Radmacher, J. P. Cleveland, M. Fritz, H. G. Hansma, and P. K. Hansma, Biophys. J. **66**(6), 2159–2165 (1994).
[3]Y. Jiao and T. E. Schäffer, Langmuir **20**(23), 10038–10045 (2004).
[4]C. Braunsmann, C. M. Hammer, J. Rheinlaender, F. E. Kruse, T. E. Schäffer, and U. Schlötzer-Schrehardt, Invest. Ophth. Vis. Sci. **53**(6), 2960–2967 (2012).
[5]H. Hertz, J. Reine Angew. Mathem. **92**, 156–171 (1882).
[6]I. N. Sneddon, Int. J. Eng. Sci. **3**(1), 47–57 (1965).
[7]D. Wang, S. Fujinami, K. Nakajima, S. Inukai, H. Ueki, A. Magario, T. Noguchi, M. Endo, and T. Nishi, Polymer **51**(12), 2455–2459 (2010).
[8]H. J. Butt, B. Cappella, and M. Kappl, Surf. Sci. Rep. **59**(1–6), 1–152 (2005).
[9]J. Domke and M. Radmacher, Langmuir **14**(12), 3320–3325 (1998).
[10]J. L. Hutter and J. Bechhoefer, Rev. Sci. Instrum. **64**(7), 1868–1873 (1993).
[11]S. S. Haykin, *Neural Networks and Learning Machines*, 3rd ed. (Prentice Hall, New York, 2009).
[12]C. Braunsmann, R. Proksch, I. Revenko, and T. E. Schäffer, Polymer **55**(1), 219–225 (2014).